

# Air-Stable and Reusable Cobalt Phosphide Nanoalloy Catalyst for Selective Hydrogenation of Furfural Derivatives

Hiroya Ishikawa, Min Sheng, Ayako Nakata,\* Kiyotaka Nakajima, Seiji Yamazoe, Jun Yamasaki, Sho Yamaguchi, Tomoo Mizugaki, and Takato Mitsudome\*



Cite This: *ACS Catal.* 2021, 11, 750–757



Read Online

ACCESS |



Metrics & More



Article Recommendations

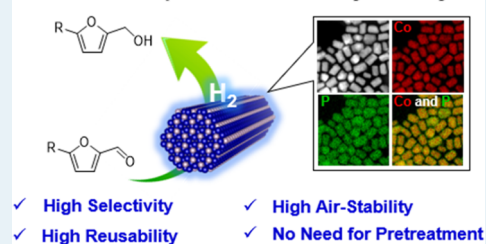


Supporting Information

**ABSTRACT:** While metal phosphides have begun to attract attention as electrocatalysts, they remain underutilized in the field of liquid-phase molecular transformations. Herein, we describe a supported cobalt phosphide nanoalloy (nano-Co<sub>2</sub>P) that functions as a highly efficient, reusable heterogeneous catalyst for the selective hydrogenation of furfural derivatives. The carbonyl moieties of several furfural derivatives were selectively hydrogenated to produce the desired products in high yields. In contrast to conventional nonprecious metal catalysts, nano-Co<sub>2</sub>P uniquely exhibited air stability, which enabled easy and safe handling and precluded the need for H<sub>2</sub> pretreatment. Infrared and density functional theory studies revealed that the highly efficient hydrogenation is due to the favorable activation of the carbonyl moiety of furfural derivatives through the backdonation to its  $\pi^*$  orbital from the Co *d*-electrons.

**KEYWORDS:** cobalt phosphide, nanoalloy, heterogeneous catalyst, hydrogenation, furfural derivative

## Cobalt Phosphide Nanoalloy Catalyst



## INTRODUCTION

The combination of a metal with other elements in nanoparticles has been recognized as a key technology in the development of new and improved catalysts. Usually, the second element is a metal, and the resulting metal–metal nanoalloy catalysts have attracted significant attention in diverse fields, such as automobile exhaust gas cleaning, oil refinery, fine chemical synthesis, and electrocatalytic and photocatalytic reactions.<sup>1–3</sup> On the other hand, metal–non-metal nanoalloys, for example, metal phosphide nanoalloys, are not as well explored. Recently, metal phosphide nanoalloys, such as nickel (Ni<sub>2</sub>P) and cobalt phosphides (Co<sub>2</sub>P), have begun to attract attention as a new family of electrocatalysts for the hydrogen evolution reaction.<sup>4</sup> These nanoalloys have also been applied to hydrotreating reactions in the petroleum industry.<sup>5</sup> However, despite their promising properties, studies on their catalytic potential for the organic syntheses of fine and bulk chemicals are rare. There are several interesting reports on nickel phosphide and cobalt phosphide in the liquid-phase hydrogenation of alkynes to alkenes,<sup>6–8</sup> nitroarenes to anilines,<sup>9,10</sup> cinnamaldehyde to cinnamyl alcohol,<sup>11</sup> and levulinic acid to  $\gamma$ -valerolactone.<sup>12,13</sup> We also showed that Ni<sub>2</sub>P and Co<sub>2</sub>P nanoalloys are highly efficient catalysts for the selective transformation of biofuranic aldehydes to diketones and the hydrogenation of nitriles to primary amines, respectively.<sup>14,15</sup> Thus, catalysis by metal phosphide nanoalloys for organic synthesis represents an exciting research area that still has unexplored possibilities. On the basis of our previous experimental results and density functional theory (DFT) calculations of the Co<sub>2</sub>P nanoalloy (nano-Co<sub>2</sub>P),<sup>14,15</sup> we

envisage that the integration of phosphorus (P) into Co nanoparticles has at least three significant merits in organic transformations. The first is the stabilization of the metallic state of the Co species. An X-ray absorption fine structure (XAFS) study showed that metal phosphide nanoalloys have a highly stable metallic state (nearly zero-valent) in air (stabilization effect), while conventional non-noble metals are highly pyrophoric. The second is the modulation of the electronic state of the Co species (ligand effect). DFT calculations revealed that P-alloying can increase the *d*-electron density of Co near the Fermi level, which favors the backdonation of electrons to the antibonding orbital of the substrate, thereby facilitating hydrogenation. The third is the precise creation of a well-defined catalytic active species (single active species) in the metal phosphide nanocrystal, which facilitates selective reactions. In contrast, conventional heterogeneous catalysts are structurally complex, that is, they contain ill-defined or irregular multiple active sites, resulting in inferior catalytic activity and selectivity. These unique properties of metal phosphide nanoalloys strongly motivated us to further investigate their catalytic potential in various organic syntheses.

Received: July 28, 2020

Revised: November 19, 2020

Published: January 1, 2021



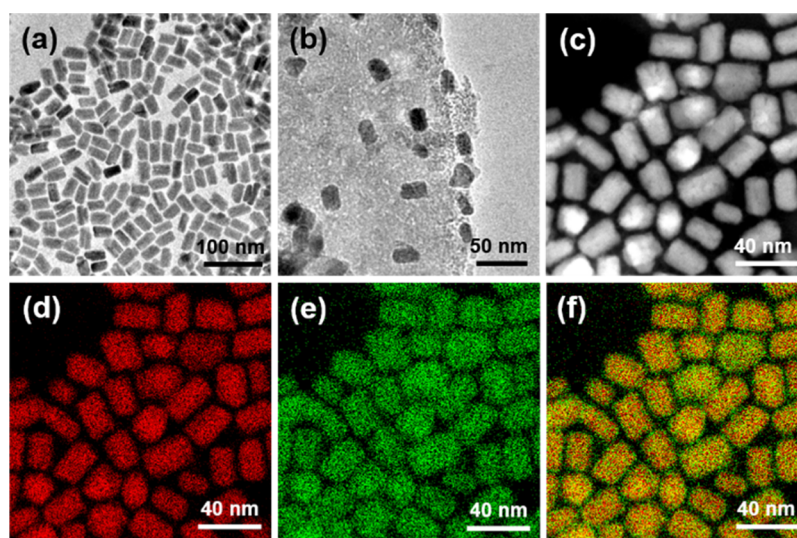


**Figure 1.** TEM images of (a) nano- $\text{Co}_2\text{P}$  and (b) nano- $\text{Co}_2\text{P}/\text{Al}_2\text{O}_3$ . (c) HAADF-STEM image of nano- $\text{Co}_2\text{P}$ . Elemental maps of (d) Co and (e) P. (f) Composition overlay image formed from (d,e).

Herein, we report that a supported nano- $\text{Co}_2\text{P}$  functions well as an efficient heterogeneous catalyst for the selective hydrogenation of furfural derivatives. Selective transformations of furfural derivatives are considerably desirable for the upgrading of biobased feedstocks because furfural derivatives are platform molecules from lignocellulosic biomass.<sup>16–18</sup> Noble-metal-based catalysts reported to date are highly active for the hydrogenation of furfural derivatives.<sup>19–21</sup> From green chemistry and economic perspectives, the replacement of precious metal catalysts with non-noble metal ones is a great challenge, and much effort has been devoted to the development of highly active non-noble metal catalysts.<sup>22–25</sup> However, all non-noble metal catalysts developed for furfural hydrogenation to date suffer from air instability (pyrophoricity). These catalysts require treatment under strictly anaerobic conditions or with  $\text{H}_2$  at high temperature before use, which severely restricts their industrial application. Therefore, the development of air-stable and reusable non-noble metal catalysts is desired. In contrast to the reported nonprecious metal catalysts, the nano- $\text{Co}_2\text{P}$  catalyst uniquely has an air-stable metallic nature that enables its easy and safe handling. Moreover, this catalyst is easily recoverable from the reaction mixture and is reusable because it retains its activity without any pretreatment. The activation state of furfural derivatives on nano- $\text{Co}_2\text{P}$  was investigated by DFT calculations.

## RESULTS AND DISCUSSION

**Catalyst Preparation and Characterization.** The well-ordered nano- $\text{Co}_2\text{P}$  was synthesized according to our previous report with some modifications.<sup>15</sup> Briefly, a mixture of 1-octadecene, hexadecylamine, and triphenyl phosphite in the presence of  $\text{CoCl}_2$  was stirred as the temperature was increased to 290 °C. Further stirring of the mixture for 2 h under Ar produced a black colloidal solution. The precipitate was collected by centrifugation and washed with acetone and chloroform to produce nano- $\text{Co}_2\text{P}$ , which was loaded onto a metal oxide support, for example,  $\text{Al}_2\text{O}_3$ , before the reaction for ease of handling and high dispersion.

The crystal structure of nano- $\text{Co}_2\text{P}$  was confirmed by X-ray diffraction. Major diffraction peaks at 40.8°, 43.5°, 52.3°, and

55.8° were observed and are attributed to the (121), (211), (002), and (320) planes, respectively, of the orthorhombic structure of the  $\text{Co}_2\text{P}$  crystal (Figure S1). A representative transmission electron microscopy (TEM) image of nano- $\text{Co}_2\text{P}$  shows the uniform formation of a nanorod structure with an average length of 32 nm and width of 18 nm (Figures 1a and S2). The high-angle annular dark-field scanning transmission electron microscopy (HAADF-STEM) image and energy-dispersive X-ray spectroscopy (EDX) elemental maps are depicted in Figures 1c–f. The constituent cobalt and phosphorus elements are homogeneously distributed in the nanorod. Elemental analysis by EDX also reveals that the Co/P atomic ratio is around 2 (Figure S3). These results clearly demonstrate the successful synthesis of nano-sized  $\text{Co}_2\text{P}$ . The high dispersion of nano- $\text{Co}_2\text{P}$  on  $\text{Al}_2\text{O}_3$  is also confirmed by the TEM image (Figure 1b).

XAFS analysis of nano- $\text{Co}_2\text{P}$  and nano- $\text{Co}_2\text{P}/\text{Al}_2\text{O}_3$  was carried out in air (Figure 2a). As we previously reported, the absorption edge energy of nano- $\text{Co}_2\text{P}$  in the Co K-edge X-ray absorption near edge structure (XANES) spectrum is similar to that of Co foil, suggesting that the Co species in  $\text{Co}_2\text{P}$  is in the metallic state.<sup>15</sup> The spectral features of nano- $\text{Co}_2\text{P}/\text{Al}_2\text{O}_3$  slightly change owing to the immobilization of nano- $\text{Co}_2\text{P}$  on

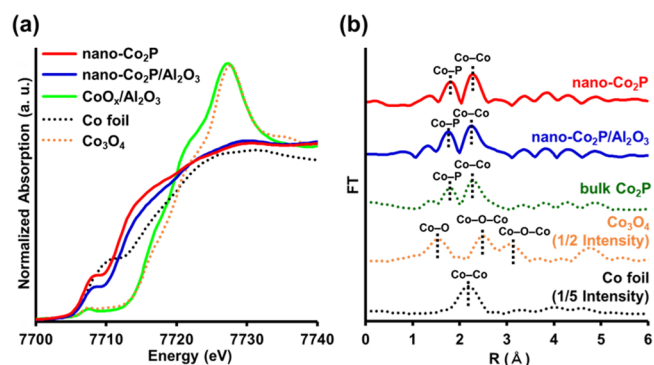


**Figure 2.** (a) Co K-edge XANES spectra of nano- $\text{Co}_2\text{P}$ , nano- $\text{Co}_2\text{P}/\text{Al}_2\text{O}_3$ , and  $\text{CoO}_x/\text{Al}_2\text{O}_3$  with Co foil and  $\text{Co}_3\text{O}_4$  as references. (b) FTs of the  $k^3$ -weighted EXAFS spectra of nano- $\text{Co}_2\text{P}$  and nano- $\text{Co}_2\text{P}/\text{Al}_2\text{O}_3$  with bulk  $\text{Co}_2\text{P}$ ,  $\text{Co}_3\text{O}_4$ , and Co foil as references.

Al<sub>2</sub>O<sub>3</sub>, albeit without the formation of the characteristic peaks of Co oxides. This indicates that the electronic states and/or local structure of nano-Co<sub>2</sub>P are affected by Al<sub>2</sub>O<sub>3</sub>. On the other hand, the absorption edge energy of Al<sub>2</sub>O<sub>3</sub>-supported cobalt (CoO<sub>x</sub>/Al<sub>2</sub>O<sub>3</sub>), a conventional catalyst prepared by the impregnation method, is much higher than those of nano-Co<sub>2</sub>P and Co foil but very similar to that of Co<sub>3</sub>O<sub>4</sub>. This suggests that di- and trivalent Co species exist in CoO<sub>x</sub>/Al<sub>2</sub>O<sub>3</sub>. These results clearly show that an air-stable zero-valent Co species is formed in nano-Co<sub>2</sub>P/Al<sub>2</sub>O<sub>3</sub> despite the instability of Co metal in air. In other words, P-alloying can afford Co species with air-stable metallic properties which is distinguished from common cobalt oxide and zero-valent cobalt metal. Figure 2b shows the Fourier-transforms extended X-ray absorption fine structure (FTs-EXAFS) spectra of nano-Co<sub>2</sub>P and nano-Co<sub>2</sub>P/Al<sub>2</sub>O<sub>3</sub>, with bulk Co<sub>2</sub>P, Co<sub>3</sub>O<sub>4</sub>, and Co foil as references. Two main peaks at 1.6–2.0 and 2.0–2.5 Å, which are attributed to Co–P and Co–Co bonds, respectively, are observed in the spectra of nano-Co<sub>2</sub>P, nano-Co<sub>2</sub>P/Al<sub>2</sub>O<sub>3</sub>, and bulk Co<sub>2</sub>P. The absence of peaks corresponding to the Co–O bond indicates that nano-Co<sub>2</sub>P and nano-Co<sub>2</sub>P/Al<sub>2</sub>O<sub>3</sub> are not oxidized in air, which is consistent with the result of the XANES analysis. The local structure of nano-Co<sub>2</sub>P was further studied by curve fitting analysis (Figure S4 and Table S1). nano-Co<sub>2</sub>P and nano-Co<sub>2</sub>P/Al<sub>2</sub>O<sub>3</sub> have longer Co–Co bonds (2.56 Å) compared with Co foil (2.49 Å) because of the existence of Co in the network of tetrahedral CoP<sub>4</sub> with vertex and edge sharing in orthorhombic Co<sub>2</sub>P. Notably, the coordination numbers of the Co–Co shell of nano-Co<sub>2</sub>P (3.5) and nano-Co<sub>2</sub>P/Al<sub>2</sub>O<sub>3</sub> (3.3) are smaller than that of bulk Co<sub>2</sub>P (4.0), which indicate that nano-Co<sub>2</sub>P and nano-Co<sub>2</sub>P/Al<sub>2</sub>O<sub>3</sub> have catalytically active unsaturated Co–Co sites on the surface. The local structure of nano-Co<sub>2</sub>P is maintained after immobilization on the Al<sub>2</sub>O<sub>3</sub> support. Therefore, the obvious change in the XANES spectrum of nano-Co<sub>2</sub>P after immobilization on Al<sub>2</sub>O<sub>3</sub> is due to the strong electronic interaction between nano-Co<sub>2</sub>P and Al<sub>2</sub>O<sub>3</sub>. The electronic states of surface Co in nano-Co<sub>2</sub>P and nano-Co<sub>2</sub>P/Al<sub>2</sub>O<sub>3</sub> were also investigated by X-ray photoelectron spectroscopy. Co 2p<sub>3/2</sub> (777.7 eV) and Co 2p<sub>1/2</sub> (792.8 eV) binding energy peaks are observed for nano-Co<sub>2</sub>P, which are very close to those of metallic Co 2p<sub>3/2</sub> (777.9 eV) and 2p<sub>1/2</sub> (793.5 eV).<sup>26</sup> These Co 2p<sub>3/2</sub> and 2p<sub>1/2</sub> peaks of nano-Co<sub>2</sub>P shift to 778.1 and 793.2 eV, respectively, after immobilization on Al<sub>2</sub>O<sub>3</sub> (Figure S5), confirming the electronic interaction between nano-Co<sub>2</sub>P and Al<sub>2</sub>O<sub>3</sub>.

**Catalytic Performance of nano-Co<sub>2</sub>P/Al<sub>2</sub>O<sub>3</sub>.** Initially, the catalytic potential of nano-Co<sub>2</sub>P/Al<sub>2</sub>O<sub>3</sub> was tested in the hydrogenation of the biomass derivative, 5-hydroxymethylfurfural (HMF), in water under 4 MPa of H<sub>2</sub> at 130 °C for 1 h without any pretreatment (Table 1). Notably, nano-Co<sub>2</sub>P/Al<sub>2</sub>O<sub>3</sub> showed high activity, and the corresponding 2,5-bis(hydroxymethyl)furan (BHMF), which is valuable as a six-carbon monomer material was obtained in 54% yield with >99% selectivity (Table 1, entry 1). A quantitative yield of BHMF was achieved by prolonging the reaction time to 4 h (Table 1, entry 2). Furthermore, nano-Co<sub>2</sub>P/Al<sub>2</sub>O<sub>3</sub> promoted hydrogenation even under milder reaction conditions (i.e., a lower H<sub>2</sub> pressure of 2 MPa and a lower reaction temperature of 80 °C), giving BHMF in >99% yield (Table 1, entry 3). Unsupported nano-Co<sub>2</sub>P also promoted the hydrogenation of HMF, although the yield of BHMF was much lower than that obtained using nano-Co<sub>2</sub>P/Al<sub>2</sub>O<sub>3</sub> (Table 1, entry 4 vs entry 1). This shows the positive effect of high dispersion of nano-Co<sub>2</sub>P

**Table 1. Hydrogenation of HMF to BHMF Using Co Catalysts<sup>a</sup>**

entry	catalyst	time (h)	conv. <sup>b</sup> (%)	sel. <sup>b</sup> (%)
1	nano-Co <sub>2</sub> P/Al <sub>2</sub> O <sub>3</sub>	1	54	>99
2	nano-Co <sub>2</sub> P/Al <sub>2</sub> O <sub>3</sub>	4	>99	>99
3 <sup>c</sup>	nano-Co <sub>2</sub> P/Al <sub>2</sub> O <sub>3</sub>	12	>99	>99
4	nano-Co <sub>2</sub> P	1	15	96
5	nano-Co <sub>2</sub> P/ZrO <sub>2</sub>	1	50	95
6	nano-Co <sub>2</sub> P/hydroxyapatite	1	40	>99
7	nano-Co <sub>2</sub> P/MgO	1	28	92
8 <sup>d</sup>	CoO <sub>x</sub> /Al <sub>2</sub> O <sub>3</sub>	1	0	-
9 <sup>e</sup>	CoO <sub>x</sub> /Al <sub>2</sub> O <sub>3</sub>	1	0	-
10	bulk Co <sub>2</sub> P	1	6	0

<sup>a</sup>Reaction conditions: HMF (0.25 mmol), H<sub>2</sub>O (3 mL). <sup>b</sup>Determined by gas chromatography–mass spectrometry (GC–MS) using an internal standard technique. <sup>c</sup>H<sub>2</sub> (2 MPa), 80 °C. <sup>d</sup>Catalyst prepared by the impregnation method. <sup>e</sup>Catalyst prepared by the deposition–precipitation method.

on Al<sub>2</sub>O<sub>3</sub>. nano-Co<sub>2</sub>P dispersed on other typical supports also gave sufficient yields of BHMF (Table 1, entries 5–7), which indicates that the type of support does not significantly affect the hydrogenation efficiency. On the other hand, conventional CoO<sub>x</sub>/Al<sub>2</sub>O<sub>3</sub> catalysts prepared by impregnation and deposition–precipitation methods did not show any catalytic activity (Table 1, entries 8 and 9). Commercially available bulk Co<sub>2</sub>P was also quite inactive in this hydrogenation reaction (Table 1, entry 10). These results clearly demonstrate that both integration of the P atom into Co and the nano-sizing of Co<sub>2</sub>P are crucial for generating a highly active Co catalyst for hydrogenation.

To confirm the occurrence of hydrogenation on nano-Co<sub>2</sub>P/Al<sub>2</sub>O<sub>3</sub>, the solid catalyst was removed by filtration after ca. 50% conversion of HMF. The filtrate was then further treated under the same reaction conditions. No additional products were formed (Scheme S1), confirming that the reaction occurs heterogeneously. After the reaction, the used nano-Co<sub>2</sub>P/Al<sub>2</sub>O<sub>3</sub> was easily recovered by simple centrifugation and reused without any loss of its catalytic activity and selectivity even after the fifth recycling experiment (Figure 3). We further investigated the reaction rate at an incomplete reaction time (1

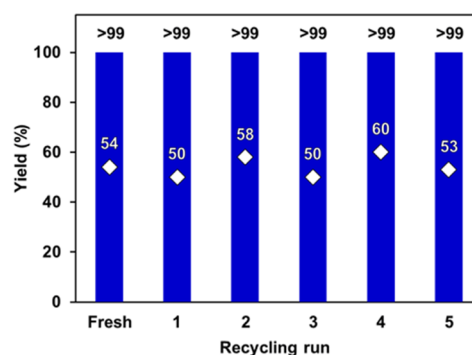


**Figure 3.** Reuse experiments of nano-Co<sub>2</sub>P/Al<sub>2</sub>O<sub>3</sub> in the hydrogenation of HMF to BHMF. Reaction conditions: nano-Co<sub>2</sub>P/Al<sub>2</sub>O<sub>3</sub> (10 mol %), HMF (0.25 mmol), H<sub>2</sub>O (3 mL), H<sub>2</sub> (4 MPa), 130 °C. Reaction time: 4 h (blue bars), 1 h (white diamonds).

h) in the recycling experiments. The yields of BHMF (diamond suit in Figure 3) obtained using the reused and fresh catalysts were similar, revealing the high durability of this catalyst. The TEM image of the used nano-Co<sub>2</sub>P/Al<sub>2</sub>O<sub>3</sub> shows that its average diameter and size distribution are similar to those of nano-Co<sub>2</sub>P/Al<sub>2</sub>O<sub>3</sub> before use, and no aggregation of nano-Co<sub>2</sub>P is observed (Figure S6). In the Co *K*-edge XANES spectrum, the absorption edge energy of the used nano-Co<sub>2</sub>P/Al<sub>2</sub>O<sub>3</sub> is almost the same as that of fresh nano-Co<sub>2</sub>P/Al<sub>2</sub>O<sub>3</sub>, suggesting that the metallic nature of the Co species is maintained during the reaction (Figure S7). Furthermore, the loading amounts of Co and P in nano-Co<sub>2</sub>P/Al<sub>2</sub>O<sub>3</sub> are almost the same before and after the reaction (Table S2). These results are consistent with the reusability of nano-Co<sub>2</sub>P/Al<sub>2</sub>O<sub>3</sub>.

Subsequently, to assess the air stability of nano-Co<sub>2</sub>P, nano-Co<sub>2</sub>P/Al<sub>2</sub>O<sub>3</sub> was exposed to air and tested in the hydrogenation of HMF. Interestingly, no catalyst deactivation was observed even after exposure to air for 72 h (Figure 4).

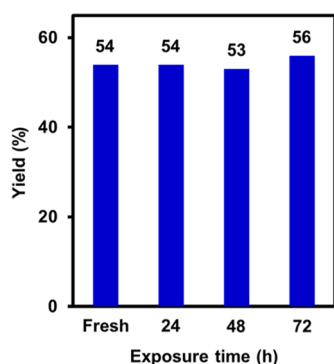


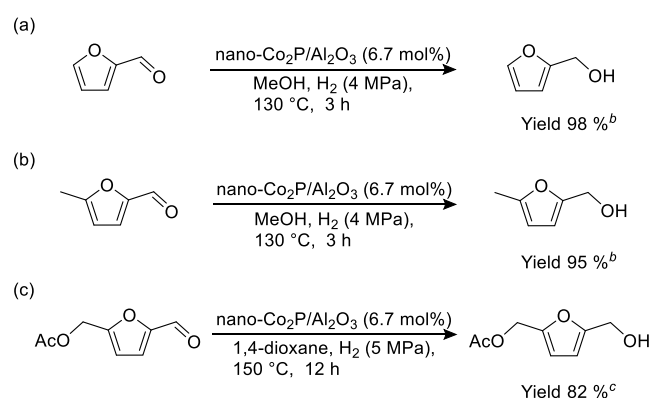
**Figure 4.** Air stability tests of nano-Co<sub>2</sub>P/Al<sub>2</sub>O<sub>3</sub> in the hydrogenation of HMF to BHMF. Reaction conditions: nano-Co<sub>2</sub>P/Al<sub>2</sub>O<sub>3</sub> (10 mol %), HMF (0.25 mmol), H<sub>2</sub>O (3 mL), H<sub>2</sub> (4 MPa), 130 °C, 1 h.

Furthermore, atomic-scale analysis using Co *K*-edge EXAFS showed that the local structure of nano-Co<sub>2</sub>P hardly changed (Figure S8), confirming that nano-Co<sub>2</sub>P has a uniquely air-stable metallic nature.

The catalytic potential of nano-Co<sub>2</sub>P in the hydrogenation of several biomass-derived furfurals (furfural, 5-methylfurfural, and 5-acetoxymethylfurfural) was further investigated. After optimizing the reaction conditions by screening various solvents (Table S3), the carbonyl moieties of furfural derivatives were selectively hydrogenated to the corresponding alcohols in high yields (Scheme 1), whereas neither furan-ring hydrogenation<sup>25,27</sup> nor hydrodeoxygenation occurred.<sup>28,29</sup> The obtained products, such as furfuryl alcohol and 5-methylfurfuryl alcohol, are useful raw materials for resins, fibers, and solvents.<sup>13,30,31</sup> nano-Co<sub>2</sub>P/Al<sub>2</sub>O<sub>3</sub> could also be operated under gram-scale conditions: 1.0 g of HMF was successfully converted to BHMF in 85% isolated yield (0.86 g) without any undesired by-products (Scheme 2).

**Rationalization of the Catalytic Behavior of nano-Co<sub>2</sub>P/Al<sub>2</sub>O<sub>3</sub>.** To obtain more insight into the unique catalysis by nano-Co<sub>2</sub>P/Al<sub>2</sub>O<sub>3</sub>, a Fourier-transform infrared (FT-IR) study of nano-Co<sub>2</sub>P/Al<sub>2</sub>O<sub>3</sub> was carried out. When furfural vapor was adsorbed on nano-Co<sub>2</sub>P/Al<sub>2</sub>O<sub>3</sub> at 25 °C, an absorption band assigned to a carbonyl bond stretching vibration appeared as a single peak at 1665 cm<sup>-1</sup> (Figure 5a). Notably, this value is much lower than that for furfural adsorbed on Al<sub>2</sub>O<sub>3</sub> at 1690 cm<sup>-1</sup> (Δ25 cm<sup>-1</sup>, Figure 5b) and

### Scheme 1. Hydrogenation of Furfural Derivatives Using nano-Co<sub>2</sub>P/Al<sub>2</sub>O<sub>3</sub><sup>a</sup>



<sup>a</sup>Reaction conditions: substrate (0.25 mmol), solvent (3 mL).

<sup>b</sup>Determined by GC-MS using an internal standard technique.

<sup>c</sup>Determined by <sup>1</sup>H NMR spectroscopy using an internal standard technique.

### Scheme 2. Gram-Scale Reaction of HMF Using nano-Co<sub>2</sub>P/Al<sub>2</sub>O<sub>3</sub>

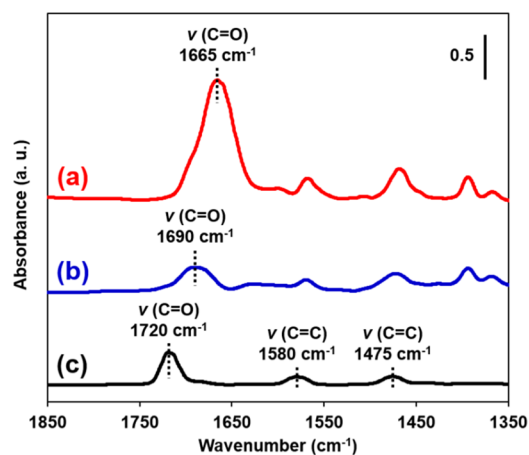
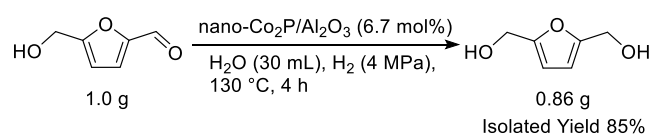


**Figure 5.** FT-IR spectra of (a) furfural-treated nano-Co<sub>2</sub>P/Al<sub>2</sub>O<sub>3</sub>, (b) furfural-treated Al<sub>2</sub>O<sub>3</sub>, and (c) pure furfural vapor.

furfural vapor at 1720 cm<sup>-1</sup> (Δ55 cm<sup>-1</sup>, Figure 5c). This large red-shift reveals that nano-Co<sub>2</sub>P can strongly activate the C=O bond of furfural. CO adsorption on nano-Co<sub>2</sub>P was also analyzed by FT-IR spectroscopy (Figure S9). CO adsorbed on nano-Co<sub>2</sub>P exhibits a peak at 2056 cm<sup>-1</sup>, which is attributed to linearly adsorbed CO on metallic Co through the back-donation of the *d*-electrons of Co to the π\* antibonding molecular orbital of CO.<sup>32</sup>

The detailed activation states of furfural on the Co<sub>2</sub>P surface were also investigated by DFT calculations. We investigated several adsorption sites on the Co<sub>2</sub>P (0001) surface (Figure S10), and the optimized structures of adsorbed furfural are shown in Figure S11. The adsorption structures can be categorized roughly into three groups, as shown in Figure 6: both the C=O bond and furan ring are adsorbed parallel to

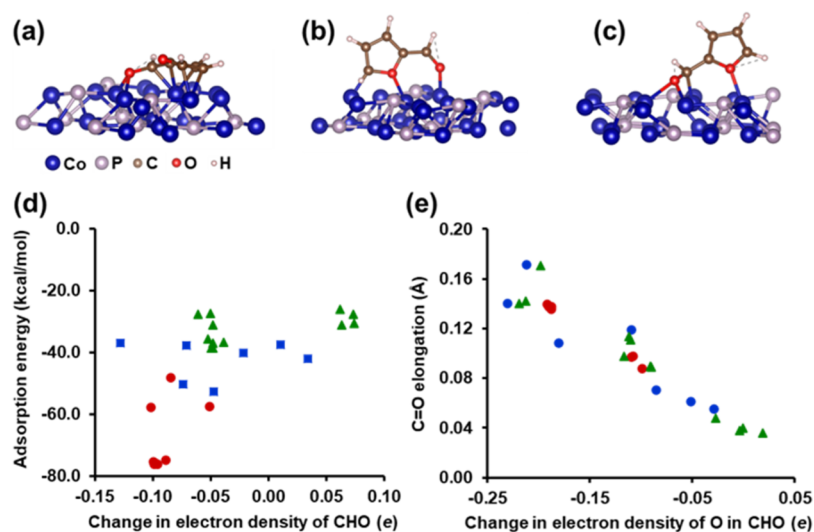


**Figure 6.** (a–c) Groups A, B, and C of the adsorption structures of furfural on the Co<sub>2</sub>P surface. Correlation of the (d) adsorption energy and (e) C=O bond elongation to the change in electron density. The red circles, blue squares, and green triangles correspond to groups A, B, and C, respectively.

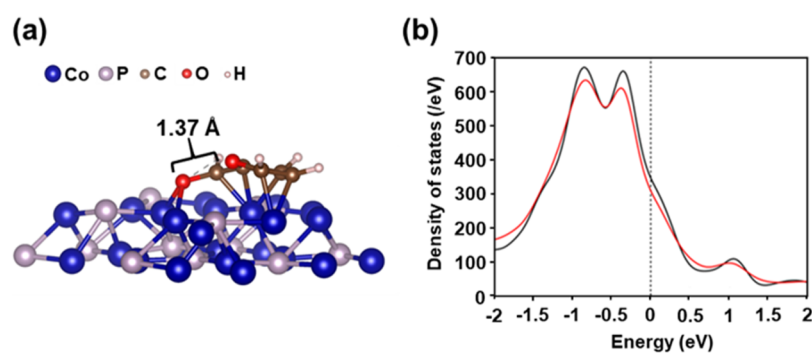


**Figure 7.** (a) Optimized structure of furfural adsorbed on the Co<sub>2</sub>P surface and (b) projected density of states of *d*-electrons on the Co<sub>2</sub>P surface (i.e., the first layer) with (red) and without (black) furfural.

the surface (group A), the O atom in C=O and a C–O bond in the furan ring are adsorbed on the surface (group B), and only C=O is strongly adsorbed on the surface (group C). The O atom in the furan ring also forms a bond to the surface in a few cases in group C. The adsorption energies,  $\Delta E = E(\text{Co}_2\text{P-furfural}) - E(\text{Co}_2\text{P}) - E(\text{furfural})$ , are summarized in Table S4. The mean adsorption energies for groups A, B, and C are  $-67.7$ ,  $-42.7$ , and  $-33.6$  kcal/mol, respectively, where a more negative energy means more stable adsorption. The bond lengths in isolated furfural and the changes caused by adsorption are given in Table S5. The C=O bond is elongated in all groups, and the mean elongation lengths for groups A, B, and C are 0.121, 0.100, and 0.092 Å, respectively. The electron distributions before and after adsorption were also investigated by Mulliken population analysis (Table S6).<sup>33</sup> The results reported in Tables S4–S6 are summarized as correlations between the adsorption energies, C=O bond elongations, and changes in electron density in Figure 6d,e, respectively. We found that the adsorption energy tends to increase as the aldehyde in furfural accepts more electrons. Moreover, the C=O bond length increases with increasing electron density of the O atom in C=O. Based on these calculated results, group A is favored over groups B and C.

The most stable adsorption structure in group A is given in Figure 7a. The C=O bond length of the furfural molecule

placed on the hollow site of nano-Co<sub>2</sub>P elongates from 1.23 to 1.37 Å upon the transfer of 0.16 electrons from nano-Co<sub>2</sub>P to furfural. Along with charge transfer, the number of *d*-electrons on the nano-Co<sub>2</sub>P surface around the Fermi level decreases, as shown in Figure 7b. These results indicate that the *d*-electrons on the nano-Co<sub>2</sub>P surface strongly activate the carbonyl moiety of furfural by enhancing the backdonation of electrons to its  $\pi^*$  orbital, which weakens the C=O bond. The activated C=O bond of furfural is then easily hydrogenated by dissociated hydrogen on the Co<sub>2</sub>P surface. We have already reported that H<sub>2</sub> dissociation on the Co<sub>2</sub>P surface is favored by electron transfer from Co<sub>2</sub>P to H<sub>2</sub>.<sup>15</sup> The results from the DFT calculations are consistent with the findings from the IR study.

## CONCLUSIONS

We report for the first time that a supported cobalt phosphide nanoalloy can serve as an air-stable and reusable heterogeneous catalyst for the selective hydrogenation of furfural derivatives. The Al<sub>2</sub>O<sub>3</sub>-supported nano-Co<sub>2</sub>P catalyst is easy to handle and does not require H<sub>2</sub> pretreatment before use. Furthermore, the supported nano-Co<sub>2</sub>P can be reused without significant loss of activity and selectivity. IR studies and DFT calculations revealed that nano-Co<sub>2</sub>P strongly activates the carbonyl moiety of furfural through the backdonation of electrons to the  $\pi^*$  orbital of the C=O moiety of furfurals, leading to the selective

hydrogenation of furfural derivatives to furfuryl alcohol derivatives.

## ■ EXPERIMENTAL SECTION

**Catalyst Preparation.** *Synthesis of nano-Co<sub>2</sub>P.* All reactions were carried out under an argon atmosphere using standard Schlenk line techniques. In a typical synthesis, 1.0 mmol of CoCl<sub>2</sub>·6H<sub>2</sub>O and 10.0 mmol of hexadecylamine were combined with 10.0 mL of 1-octadecene and 10.0 mmol of triphenyl phosphite in a Schlenk flask. The system was heated to 150 °C to remove low-boiling-point impurities. The temperature was then increased to 290 °C and maintained for 2 h. Afterward, the mixture was cooled to room temperature. The black product was isolated by precipitation with acetone. To remove as much organics as possible, redispersion and precipitation cycles using chloroform and acetone were continued until the supernatant liquid was transparent. The obtained powder was dried in vacuum overnight.

*Preparation of nano-Co<sub>2</sub>P/Support.* Typically, 37.2 mg of nano-Co<sub>2</sub>P was dispersed in 100 mL of *n*-hexane and stirred with 1.0 g of Al<sub>2</sub>O<sub>3</sub> at room temperature. The obtained powder was dried in vacuum overnight to produce nano-Co<sub>2</sub>P/Al<sub>2</sub>O<sub>3</sub> as a gray powder. The same procedure was used to prepare the other nano-Co<sub>2</sub>P/support catalysts.

*Preparation of CoO<sub>x</sub>/Al<sub>2</sub>O<sub>3</sub> by Impregnation Method.* CoCl<sub>2</sub>·6H<sub>2</sub>O (0.5 mmol) was dissolved in acetone (50 mL). Al<sub>2</sub>O<sub>3</sub> (1.0 g) was added, and the mixture was stirred for 30 min at room temperature. Acetone was removed by evaporation under reduced pressure, and the obtained powder was dried at 110 °C overnight. The dried powder was calcined in air at 500 °C for 3 h to produce CoO<sub>x</sub>/Al<sub>2</sub>O<sub>3</sub>.

*Preparation of CoO<sub>x</sub>/Al<sub>2</sub>O<sub>3</sub> by Deposition–Precipitation Method.* Al<sub>2</sub>O<sub>3</sub> (1.0 g) was soaked in 50 mL of an aqueous solution of CoCl<sub>2</sub> (10 mM). The pH was then adjusted to 8.5 with a solution of NaOH (0.1 M). After stirring the mixture for 6 h at room temperature, the obtained solid was filtered, washed with deionized water, and dried in vacuum at room temperature, producing CoO<sub>x</sub>/Al<sub>2</sub>O<sub>3</sub>.

**Typical Reaction Procedure.** The typical reaction procedure for the hydrogenation of HMF to BHMF using nano-Co<sub>2</sub>P/Al<sub>2</sub>O<sub>3</sub> was as follows. nano-Co<sub>2</sub>P/Al<sub>2</sub>O<sub>3</sub> powder was placed in a 50 mL stainless steel autoclave with a Teflon inner cylinder. HMF (0.25 mmol) and distilled water (3 mL) were subsequently added. The reaction mixture was stirred vigorously at 130 °C under 4 MPa of H<sub>2</sub>. After the reaction, dimethyl sulfone (internal standard) and MeOH were added to the reaction mixture, and then, the catalyst was separated by centrifugation. The reaction solution was analyzed by GC–MS to determine the conversion and yield. GC–MS was performed using a Shimadzu GCMS-QP2010 SE gas chromatograph–mass spectrometer equipped with a capillary column (InertCap WAX-HT, GL Sciences, 30 m × 0.25 mm i.d., 0.25 μm). The column oven temperature started from 120 °C (3-min hold) and was then increased to 200 °C at a heating rate of 20 °C/min. Other conditions were as follows: column flow rate (He carrier): 1.22 mL/min; split ratio: 32:1; injector temperature: 250 °C; and interface temperature: 250 °C.

**Recycling Experiments.** After the reaction, nano-Co<sub>2</sub>P/Al<sub>2</sub>O<sub>3</sub> was removed by centrifugation, and the yield was determined by GC–MS analysis. The spent catalyst was washed with water and 2-propanol for the reuse experiments without any other pretreatment.

**Gram-Scale Reaction.** The gram-scale reaction of HMF was performed in a 300 mL stainless steel autoclave with a Teflon inner cylinder at 130 °C under 4 MPa of H<sub>2</sub> for 4 h. After the reaction, nano-Co<sub>2</sub>P/Al<sub>2</sub>O<sub>3</sub> was filtered to separate the liquid phase from the solid catalyst. The solvent was evaporated, and the residue was subjected to silica gel column chromatography (chloroform/methanol = 93/7) to produce isolated BHMF, which was identified by GC–MS and <sup>1</sup>H and <sup>13</sup>C NMR.

## ■ ASSOCIATED CONTENT

### Supporting Information

The Supporting Information is available free of charge at <https://pubs.acs.org/doi/10.1021/acscatal.0c03300>.

General experimental details, characterization of catalysts, hot filtration experiment, effect of solvents, DFT calculation details, and product identification (PDF)

## ■ AUTHOR INFORMATION

### Corresponding Authors

**Ayako Nakata** – First-Principles Simulation Group, Nano-Theory Field, International Center for Materials Nanoarchitectonics (WPI-MANA), National Institute for Materials Science (NIMS), Tsukuba, Ibaraki 305-0044, Japan; [orcid.org/0000-0002-3311-6283](https://orcid.org/0000-0002-3311-6283); Email: [NAKATA.ayako@nims.go.jp](mailto:NAKATA.ayako@nims.go.jp)

**Takato Mitsudome** – Department of Materials Engineering Science, Graduate School of Engineering Science, Osaka University, Toyonaka, Osaka 560-8531, Japan; [orcid.org/0000-0002-0924-5616](https://orcid.org/0000-0002-0924-5616); Email: [mitsudom@cheng.es.osaka-u.ac.jp](mailto:mitsudom@cheng.es.osaka-u.ac.jp)

### Authors

**Hiroya Ishikawa** – Department of Materials Engineering Science, Graduate School of Engineering Science, Osaka University, Toyonaka, Osaka 560-8531, Japan

**Min Sheng** – Department of Materials Engineering Science, Graduate School of Engineering Science, Osaka University, Toyonaka, Osaka 560-8531, Japan

**Kiyotaka Nakajima** – Institute for Catalysis, Hokkaido University, Kita-ku, Sapporo 001-0021, Japan; [orcid.org/0000-0002-3774-3209](https://orcid.org/0000-0002-3774-3209)

**Seiji Yamazoe** – Department of Chemistry, Tokyo Metropolitan University, Hachioji, Tokyo 192-0397, Japan; [orcid.org/0000-0002-8382-8078](https://orcid.org/0000-0002-8382-8078)

**Jun Yamasaki** – Research Center for Ultra-High Voltage Electron Microscopy, Osaka University, Ibaraki, Osaka 567-0047, Japan

**Sho Yamaguchi** – Department of Materials Engineering Science, Graduate School of Engineering Science, Osaka University, Toyonaka, Osaka 560-8531, Japan; [orcid.org/0000-0002-0014-3218](https://orcid.org/0000-0002-0014-3218)

**Tomoo Mizugaki** – Department of Materials Engineering Science, Graduate School of Engineering Science, Osaka University, Toyonaka, Osaka 560-8531, Japan; [orcid.org/0000-0001-5701-7530](https://orcid.org/0000-0001-5701-7530)

Complete contact information is available at: <https://pubs.acs.org/doi/10.1021/acscatal.0c03300>

## Author Contributions

The manuscript was written through the contributions of all authors. All authors have given approval to the final version of the manuscript.

## Notes

The authors declare no competing financial interest.

## ACKNOWLEDGMENTS

This work was supported by the Japan Society for the Promotion of Science (JSPS) KAKENHI Grant nos. 26105003, 17H03457, 18H01790, 17H05224, and 20H02523. This study was partially supported by the Cooperative Research Program of the Institute for Catalysis, Hokkaido University (20B1027). A part of this work was supported by the “Nanotechnology Platform” program at Hokkaido University (A-20-HK-0011) and Nanotechnology Open Facilities in Osaka University (A-19-OS-0060) of the Ministry of Education, Culture, Sports, Science and Technology (MEXT), Japan. The DFT calculations were performed on the Numerical Materials Simulator at NIMS, and the computer resource was offered under the category of General Projects by the Research Institute for Information Technology, Kyushu University. The authors thank Dr. Toshiaki Ina (SPRING-8) for the XAFS measurements (2019A1390, 2019A1649, and 2019B1560) and Ryo Ota of Hokkaido University for the STEM analysis.

## REFERENCES

- (1) Fang, H.; Yang, J.; Wen, M.; Wu, Q. Nanoalloy Materials for Chemical Catalysis. *Adv. Mater.* **2018**, *30*, 1705698.
- (2) Bing, Y.; Liu, H.; Zhang, L.; Ghosh, D.; Zhang, J. Nanostructured Pt-Alloy Electrocatalysts for PEM Fuel Cell Oxygen Reduction Reaction. *Chem. Soc. Rev.* **2010**, *39*, 2184–2202.
- (3) Gilroy, K. D.; Ruditskiy, A.; Peng, H.-C.; Qin, D.; Xia, Y. Bimetallic Nanocrystals: Syntheses, Properties, and Applications. *Chem. Rev.* **2016**, *116*, 10414–10472.
- (4) Shi, Y.; Zhang, B. Recent Advances in Transition Metal Phosphide Nanomaterials: Synthesis and Applications in Hydrogen Evolution Reaction. *Chem. Soc. Rev.* **2016**, *45*, 1529–1541.
- (5) Oyama, S. T. Novel Catalysts for Advanced Hydroprocessing: Transition Metal Phosphides. *J. Catal.* **2003**, *216*, 343–352.
- (6) Carencio, S.; Leyva-Pérez, A.; Concepción, P.; Boissière, C.; Mézailles, N.; Sanchez, C.; Corma, A. Nickel Phosphide Nanocatalysts for the Chemoselective Hydrogenation of Alkynes. *Nano Today* **2012**, *7*, 21–28.
- (7) Albani, D.; Karajovic, K.; Tata, B.; Li, Q.; Mitchell, S.; López, N.; Pérez-Ramírez, J. Ensemble Design in Nickel Phosphide Catalysts for Alkyne Semi-Hydrogenation. *ChemCatChem* **2019**, *11*, 457–464.
- (8) Chen, Y.; Li, C.; Zhou, J.; Zhang, S.; Rao, D.; He, S.; Wei, M.; Evans, D. G.; Duan, X. Metal Phosphides Derived from Hydrotalcite Precursors toward the Selective Hydrogenation of Phenylacetylene. *ACS Catal.* **2015**, *5*, 5756–5765.
- (9) Yang, S.; Peng, L.; Oveisi, E.; Bulut, S.; Sun, D. T.; Asgari, M.; Trukhina, O.; Queen, W. L. MOF-Derived Cobalt Phosphide/Carbon Nanocubes for Selective Hydrogenation of Nitroarenes to Anilines. *Chem.—Eur. J.* **2018**, *24*, 4234–4238.
- (10) Gao, R.; Pan, L.; Wang, H.; Zhang, X.; Wang, L.; Zou, J.-J. Ultradispersed Nickel Phosphide on Phosphorus-Doped Carbon with Tailored d-Band Center for Efficient and Chemoselective Hydrogenation of Nitroarenes. *ACS Catal.* **2018**, *8*, 8420–8429.
- (11) Gao, R.; Pan, L.; Wang, H.; Yao, Y.; Zhang, X.; Wang, L.; Zou, J. J. Breaking Trade-Off between Selectivity and Activity of Nickel-Based Hydrogenation Catalysts by Tuning Both Steric Effect and d-Band Center. *Adv. Sci.* **2019**, *6*, 1900054.
- (12) Feng, H.-J.; Li, X.-C.; Qian, H.; Zhang, Y.-F.; Zhang, D.-H.; Zhao, D.; Hong, S.-G.; Zhang, N. Efficient and Sustainable

Hydrogenation of Levulinic-Acid to Gamma-Valerolactone in Aqueous Solution over Acid-Resistant CePO<sub>4</sub>/Co<sub>2</sub>P Catalysts. *Green Chem.* **2019**, *21*, 1743–1756.

- (13) Yu, Z.; Meng, F.; Wang, Y.; Sun, Z.; Liu, Y.; Shi, C.; Wang, W.; Wang, A. Catalytic Transfer Hydrogenation of Levulinic Acid to  $\gamma$ -Valerolactone over Ni<sub>3</sub>P-CePO<sub>4</sub> Catalysts. *Ind. Eng. Chem. Res.* **2020**, *59*, 7416–7425.

- (14) Fujita, S.; Nakajima, K.; Yamasaki, J.; Mizugaki, T.; Jitsukawa, K.; Mitsudome, T. Unique Catalysis of Nickel Phosphide Nanoparticles to Promote the Selective Transformation of Biofuran Aldehydes into Diketones in Water. *ACS Catal.* **2020**, *10*, 4261–4267.

- (15) Mitsudome, T.; Sheng, M.; Nakata, A.; Yamasaki, J.; Mizugaki, T.; Jitsukawa, K. A Cobalt Phosphide Catalyst for the Hydrogenation of Nitriles. *Chem. Sci.* **2020**, *11*, 6682–6689.

- (16) Alonso, D. M.; Bond, J. Q.; Dumesic, J. A. Catalytic Conversion of Biomass to Biofuels. *Green Chem.* **2010**, *12*, 1493–1513.

- (17) Nakagawa, Y.; Tamura, M.; Tomishige, K. Catalytic Reduction of Biomass-Derived Furanic Compounds with Hydrogen. *ACS Catal.* **2013**, *3*, 2655–2668.

- (18) Chen, S.; Wojcieszak, R.; Dumeignil, F.; Marceau, E.; Royer, S. How Catalysts and Experimental Conditions Determine the Selective Hydroconversion of Furfural and 5-Hydroxymethylfurfural. *Chem. Rev.* **2018**, *118*, 11023–11117.

- (19) Chen, J.; Lu, F.; Zhang, J.; Yu, W.; Wang, F.; Gao, J.; Xu, J. Immobilized Ru Clusters in Nanosized Mesoporous Zirconium Silica for the Aqueous Hydrogenation of Furan Derivatives at Room Temperature. *ChemCatChem* **2013**, *5*, 2822–2826.

- (20) Chatterjee, M.; Ishizaka, T.; Kawanami, H. Selective Hydrogenation of 5-Hydroxymethylfurfural to 2,5-Bis-(hydroxymethyl)furan using Pt/MCM-41 in an Aqueous Medium: A Simple Approach. *Green Chem.* **2014**, *16*, 4734–4739.

- (21) Tamura, M.; Tokonami, K.; Nakagawa, Y.; Tomishige, K. Rapid Synthesis of Unsaturated Alcohols under Mild Conditions by Highly Selective Hydrogenation. *Chem. Commun.* **2013**, *49*, 7034–7036.

- (22) Zhu, Y.; Kong, X.; Yin, J.; You, R.; Zhang, B.; Zheng, H.; Wen, X.; Zhu, Y.; Li, Y.-W. Covalent-Bonding to Irreducible SiO<sub>2</sub> Leads to High-Loading and Atomically Dispersed Metal Catalysts. *J. Catal.* **2017**, *353*, 315–324.

- (23) Ma, Y.; Xu, G.; Wang, H.; Wang, Y.; Zhang, Y.; Fu, Y. Cobalt Nanocluster Supported on ZrRE<sub>n</sub>O<sub>x</sub> for the Selective Hydrogenation of Biomass Derived Aromatic Aldehydes and Ketones in Water. *ACS Catal.* **2018**, *8*, 1268–1277.

- (24) Watari, R.; Matsumoto, N.; Kuwata, S.; Kayaki, Y. Distinct Promotive Effects of 1,8-Diazabicyclo[5.4.0]undec-7-ene (DBU) on Polymer Supports in Copper-Catalyzed Hydrogenation of C=O Bonds. *ChemCatChem* **2017**, *9*, 4501–4507.

- (25) Zhu, Y.; Kong, X.; Zheng, H.; Ding, G.; Zhu, Y.; Li, Y.-W. Efficient Synthesis of 2,5-Dihydroxymethylfuran and 2,5-Dimethylfuran from 5-Hydroxymethylfurfural using Mineral-Derived Cu Catalysts as Versatile Catalysts. *Catal. Sci. Technol.* **2015**, *5*, 4208–4217.

- (26) Wagner, C. D.; Riggs, W. M.; Davis, L. E.; Mouler, J. F.; Muilenberg, G. E. *Handbook of X-Ray Photoelectron Spectroscopy*; Perkin-Elmer Corp.: Eden Prairie, MN, 1979.

- (27) Alamillo, R.; Tucker, M.; Chia, M.; Pagán-Torres, Y.; Dumesic, J. The Selective Hydrogenation of Biomass-Derived 5-Hydroxymethylfurfural using Heterogeneous Catalysts. *Green Chem.* **2012**, *14*, 1413–1419.

- (28) Kong, X.; Zhu, Y.; Zheng, H.; Dong, F.; Zhu, Y.; Li, Y.-W. Switchable Synthesis of 2,5-Dimethylfuran and 2,5-Dihydroxymethyltetrahydrofuran from 5-Hydroxymethylfurfural over Raney Ni Catalyst. *RSC Adv.* **2014**, *4*, 60467–60472.

- (29) Kumalaputri, A. J.; Bottari, G.; Erne, P. M.; Heeres, H. J.; Barta, K. Tunable and Selective Conversion of 5-HMF to 2,5-Furandimethanol and 2,5-Dimethylfuran over Copper-Doped Porous Metal Oxides. *ChemSusChem* **2014**, *7*, 2266–2275.

- (30) Yan, K.; Wu, G.; Lafleur, T.; Jarvis, C. Production, Properties and Catalytic Hydrogenation of Furfural to Fuel Additives and Value-Added Chemicals. *Renewable Sustainable Energy Rev.* **2014**, *38*, 663–676.

(31) Mariscal, R.; Maireles-Torres, P.; Ojeda, M.; Sádaba, I.; López Granados, M. Furfural: A Renewable and Versatile Platform Molecule for the Synthesis of Chemicals and Fuels. *Energy Environ. Sci.* **2016**, *9*, 1144–1189.

(32) Khassin, A. A.; Yurieva, T. M.; Kaichev, V. V.; Bukhtiyarov, V. I.; Budneva, A. A.; Paukshtis, E. A.; Parmon, V. N. Metal–Support Interactions in Cobalt-Aluminum Co-Precipitated Catalysts: XPS and CO Adsorption Studies. *J. Mol. Catal. A: Chem.* **2001**, *175*, 189–204.

(33) Mulliken, R. S. Electronic Population Analysis on LCAO–MO Molecular Wave Functions I. *J. Chem. Phys.* **1955**, *23*, 1833–1840.